AGU PUBLICATIONS

Geochemistry, Geophysics, Geosystems

RESEARCH ARTICLE
10.1002/2015GC006058

Special Section:
Subduction processes in Central America with an emphasis on CRISP results

# Paleomagnetic constraints on the tectonic evolution of the Costa Rican subduction zone: New results from sedimentary successions of IODP drill sites from the Cocos Ridge

**Yong-Xiang Li[1], Xixi Zhao[2,3], Luigi Jovane[4], Katerina E. Petronotis[5], Zheng Gong[1], and Siyi Xie[1]**

[1]State Key Laboratory for Mineral Deposits Research, School of Earth Sciences and Engineering, Institute of Geophysics and Geodynamics, Nanjing University, Nanjing, China, [2]State Key Laboratory of Marine Geology, Tongji University, Shanghai, China, [3]Department of Earth and Planetary Sciences, University of California, Santa Cruz, Santa Cruz, California, USA, [4]Instituto Oceanográfico, Universidade de São Paulo, São Paulo, Brazil, [5]International Ocean Discovery Program, Texas A&M University, College Station, Texas, USA

**Abstract** The near-flat subduction of the Cocos Ridge (CR) along the Middle American Trench (MAT) plays a pivotal role in governing the geodynamic evolution of the central American convergent margin. Elucidating the onset of its subduction is essential to understand the tectonic evolution and seismogenesis of the Costa Rican convergent margin, a typical erosive convergent margin and modern example of a flat-slab subduction. Initial subduction of the CR has been previously investigated by examining upper plate deformation that was inferred to have resulted from the initial CR subduction. However, little attention has been paid to the extensive sedimentary archives on the CR that could hold important clues to the initial CR subduction. Drilling on the CR during IODP Expedition 344 discovered a pronounced sedimentary hiatus at Site U1381. Here we present paleomagnetic and rock magnetic results of the Cenozoic sedimentary sequences at this site that bracket the hiatus between ca. 9.61 and 1.52 Ma. We also examine the areal extent, timing, and geologic significance of the hiatus by analyzing sedimentary records from five other ODP/IODP sites on CR and Cocos plate. The analyses show that the hiatus appears to be regional and the presence/absence of the sedimentary hiatus at different locations on CR implies a link to the onset of CR shallow subduction, as a result of either bottom current erosion or CR buckling upon its initial collision at the MAT. Records directly from CR thus provide a new window to unraveling the geodynamic evolution of the central American margin.

**Key Points:**
- A paleomagnetic study is performed on fully oriented IODP cores drilled from the Cocos Ridge
- A sedimentary hiatus is recognized and is constrained at 1.52 and 9.61 Ma with paleomagnetic data
- The hiatus appears regional and is linked to the initial shallow subduction of the Cocos Ridge

**Supporting Information:**
- Supporting Information S1

**Correspondence to:**
Y.-X. Li,
yxli@nju.edu.cn

**Citation:**
Li, Y.-X., X. Zhao, L. Jovane, K. E. Petronotis, Z. Gong, and S. Xie (2015), Paleomagnetic constraints on the tectonic evolution of the Costa Rican subduction zone: New results from sedimentary successions of IODP drill sites from the Cocos Ridge, *Geochem. Geophys. Geosyst.*, *16*, 4479–4493, doi:10.1002/2015GC006058.

Received 13 AUG 2015
Accepted 5 DEC 2015
Accepted article online 14 DEC 2015
Published online 31 DEC 2015
Corrected 25 JAN 2016

This article was corrected on 25 JAN 2016. See the end of the full text for details.



## 1. Introduction

Offshore of the Osa Peninsula of Costa Rica is a sediment-dominated subduction zone formed by subduction of the Cocos plate beneath Costa Rica [e.g., *Vannucchi et al.*, 2006]. One of the most unique features of the Costa Rican convergent margin is the near-flat subduction of the Cocos Ridge (CR) at the Middle American Trench (MAT). In fact, the subduction of the CR beneath southern Costa Rica at the MAT has intrigued geoscientists for decades [e.g., *Lonsdale and Klitgord*, 1978; *Drummond et al.*, 1995; *Corrigan et al.*, 1990; *Fisher et al.*, 2004; *LaFemina et al.*, 2009; *Vannucchi et al.*, 2001, 2013; *Kobayashi et al.*, 2014] and it is widely accepted that the CR subduction plays a critical role in governing the geodynamic evolution of the central American margin.

The ~1000 km long, ~200–300 km wide CR (Figure 1) is an aseismic ridge that was formed when the Cocos plate drifted over the Galapagos hot spot [*Barckhausen et al.*, 2001]. The crust of the CR is anomalously thick (>20 km) [*Walther*, 2003], which is about 3 times that of normal oceanic crust thickness, making it relatively buoyant. The CR is subducting almost orthogonally into the MAT at a low angle of ~3°–10° [*Protti et al.*, 1995] and at a rate of 8.5 cm/yr [*Morell et al.*, 2012] to 9.5 cm/yr [*DeMets et al.*, 1994] (Figure 1). Shallow subduction of the CR has a profound impact on the central American convergent margin and has given rise to dramatic deformation of the overriding Caribbean Plate, including significant crustal shortening, segmentation of the upper plate, and widespread uplift of coastal Costa Rica from Nicoya Peninsula to Osa Peninsula (Figure 1) extending more than 100 km inland from the trench [*Fisher et al.*, 2004; *LaFemina et al.*, 2009; *Sak et al.*, 2009; *Gardner et al.*, 2013; *Kobayashi et al.*, 2014]. In addition, because the CR is about 2.5 km higher than the surrounding seafloor of the Cocos Plate, shallow subduction of the CR is highly effective in eroding the overlying plate, leading to dramatic fore-arc subsidence and landward trench retreat of the Costa Rican convergent margin [*Ranero and von Huene*, 2000; *Vannucchi et al.*, 2001, 2013]. Furthermore, the shallow

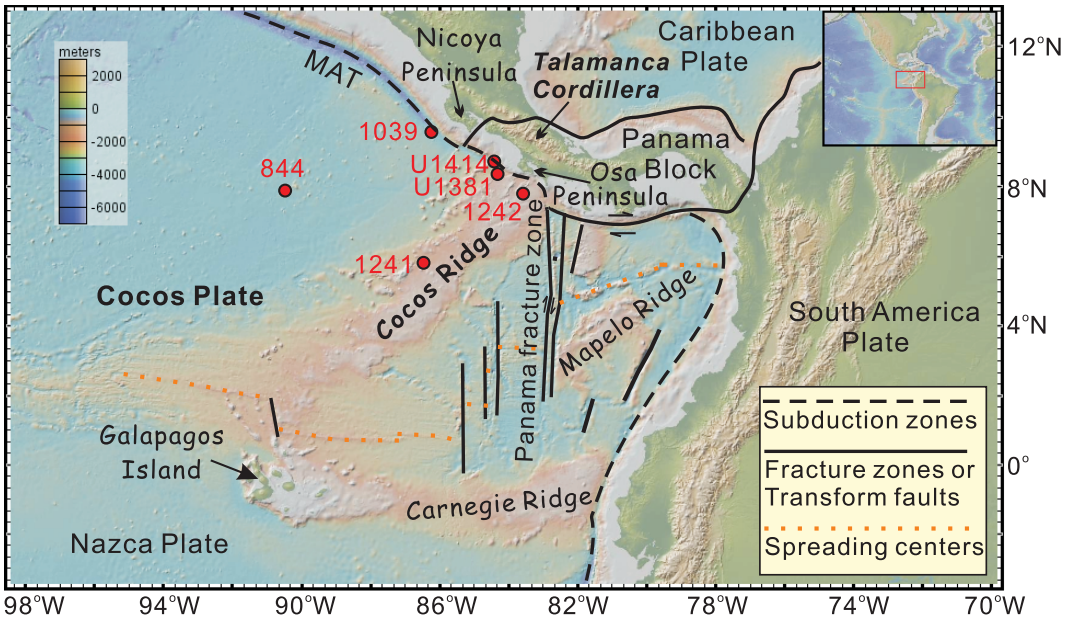


**Figure 1.** Digital elevation map showing the general plate tectonic setting of Central America and the major ODP and IODP sites on and near the aseismic Cocos Ridge [after *Vannucchi et al.*, 2013]. MAT, Middle American Trench.

subduction of the CR triggers frequent and sometimes large ($M_w > 7$) earthquakes along the margin [*Protti et al.*, 1995; *Newman et al.*, 2002; *Vannucchi et al.*, 2012; *Harris et al.*, 2013] that pose a significant seismic hazard for the communities in that region.

The CR subduction is interesting also because it provides a rare opportunity to examine a modern example of at least one type of flat-slab subduction, a tectonic model that has been frequently invoked to explain the geodynamics of subduction zones in the geologic past, such as the Late Cretaceous to Paleogene Laramide Orogeny in the western North America [*Dickinson and Snyder*, 1978] and the widespread Mesozoic magmatism in southeast China [*Li and Li*, 2007]. Although much has been learned about the CR subduction, our knowledge is largely based on investigations of the deformation in the upper plate [e.g., *Gardner et al.*, 1992; *Abratis and Wörner*, 2001; *Gräfe et al.*, 2002], probably because of the relatively easier access. Little attention has been paid to the extensive sedimentary records directly associated with the subducting CR, which may hold important clues to the evolution of the Costa Rican margin.

Integrated Ocean Drilling Program (IODP) Expeditions 334 and 344 conducted drilling offshore the Osa Peninsula of Costa Rica to understand the processes that control nucleation and seismic rupture of large earthquakes at the Costa Rican convergent margin [*Vannucchi et al.*, 2012; *Harris et al.*, 2013]. Drilling not only recovered sediments from the upper plate but also sampled sediments from the subducting CR. Sites U1381 and U1414 were drilled at the summit and the flank of the CR, respectively (Figure 1). Shipboard analyses show that there is a sedimentary hiatus at Site U1381, whereas sedimentation at Site U1414 is interpreted to be continuous [*Harris et al.*, 2013].

Here we present new paleomagnetic and rock magnetic results of samples from Site U1381 to establish a magnetostratigraphy for the cores. We also compile sedimentary records from four Ocean Drilling Program (ODP)/IODP sites on the CR (Sites 1241, 1242, U1381, and U1414) as well as two ODP sites on the Cocos Plate and near the CR (Sites 844 and 1039) (Figure 1) to examine whether the sedimentary hiatus observed at Site U1381 occurred at a regional scale on the CR. We subsequently combine the magnetostratigraphic constraints on the timing of the hiatus and the discovery of the apparently regional occurrence of the hiatus to investigate implications for the tectonic evolution of the Costa Rican margin.

## 2. Background Information of Sites

Several ODP/IODP sites were drilled on the CR and on the nearby Cocos Plate (Figure 1). Sites U1381 and U1414 were drilled during IODP Expeditions 334 and 344 [*Vannucchi et al.*, 2012; *Harris et al.*, 2013] from the

**Table 1.** Locations of ODP/IODP Sites

| Site | Coordinates | | Reference |
|---|---|---|---|
| 844 | N 7°55.279′ | W 90°28.846′ | *Mayer et al.* [1992] |
| 1241 | N 5°50.57′ | W 86°26.676′ | *Mix et al.* [2003] |
| 1242 | N 7°51.352′ | W 83°36.418′ | *Mix et al.* [2003] |
| U1381 | N 8°25.7027′ | W 84°9.48′ | *Harris et al.* [2013] |
| U1414 | N 8°30.2304′ | W 84°13.5298′ | *Harris et al.* [2013] |
| 1039 | N 9°38′ | W 86°13′ | *Morris et al.* [2006] and *Silver et al.* [2000] |

northeastern part of CR. Sites 1241 and 1242 were drilled during ODP Leg 202 [*Mix et al.*, 2003] from the middle and northeastern part of CR. Site 844 of ODP Leg 138 [*Mayer et al.*, 1992] and Site 1039 of ODP Leg 170 [*Ibaraki*, 2000; *Morris et al.*, 2006] were drilled on the Cocos Plate near the CR at proximal and distal locations with respect to the MAT (Figure 1). The locations of these sites are shown in Figure 1 and their coordinates are summarized in Table 1. Also, stratigraphic columns of these sites are compiled and are arranged according to their distance to the MAT in Figures 2a–2f.

### 2.1. Sites U1381 and U1414

Site U1381 is situated at 8°25.7′N, 84°9.5′W on the CR (Figure 1). Because the Cocos Plate is moving to the northeast [*Hey et al.*, 1977], Site U1381 was located close to the equator and at a shallower water depth near the Galapagos hot spot in its early history according to a tectonic reconstruction of the Cocos Plate [*Pisias et al.*, 1995]. Therefore, Site U1381 has been in the Northern Hemisphere since its formation.

Holes U1381A and U1381B were cored during Expedition 334 with the IODP rotary core barrel (RCB) system, resulting in severely disturbed sediments [*Vannucchi et al.*, 2012]. Hole U1381C was cored during Expedition 344 with the advanced piston corer (APC) system, using nonmagnetic core barrels. Hole U1381C penetrated through the 103.55 m thick sedimentary sequence and reached the basaltic basement [*Harris et al.*, 2013] (Figures 2d and 3a). The basaltic basement was cored with the extended core barrel (XCB) system for 0.33 m. The sediments cored with the APC had minimal disturbance. In addition, the upper 84 m of sediments (i.e., Cores 1H–9H, Figure 3a) were fully oriented, which makes them most suitable for paleomagnetic investigations. The recovered sediments consist of three lithologic units. The basal unit is a 0.35 m thick

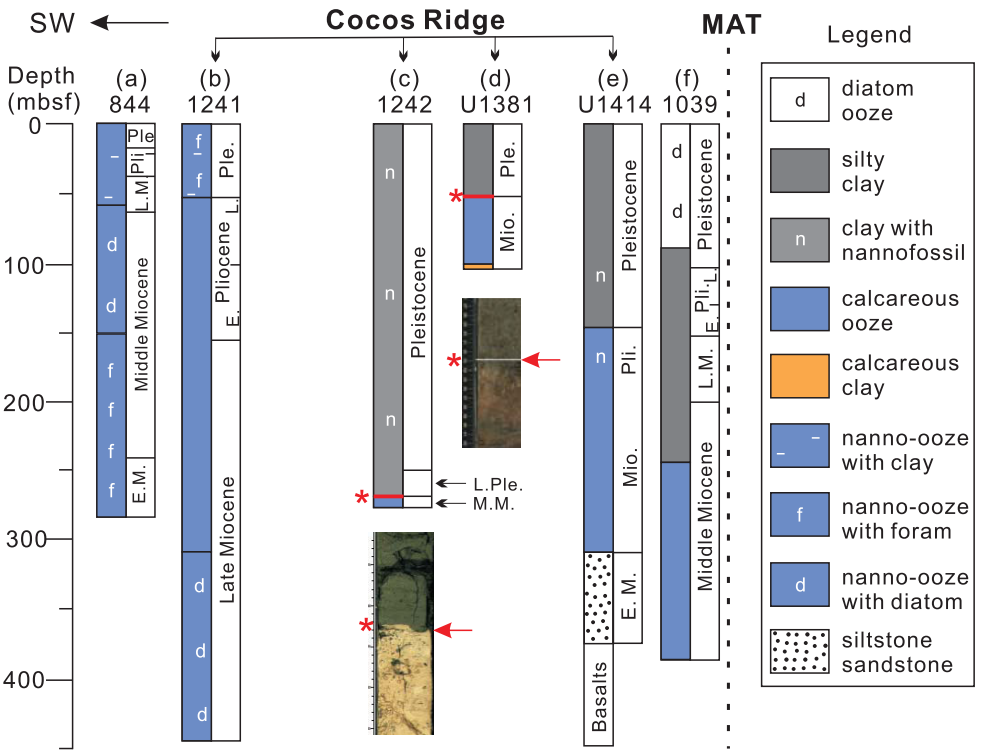


**Figure 2.** (a–f) Sedimentary records from ODP/IODP sites drilled at the Cocos Ridge (CR) and the Cocos Plate (see Figure 1 for site locations). mbsf = meters below seafloor; E.M/M.M./L.M.= early/middle/late Miocene; Pli./Ple. = Pliocene/Pleistocene. Red lines/asterisks/arrows mark hiatuses.

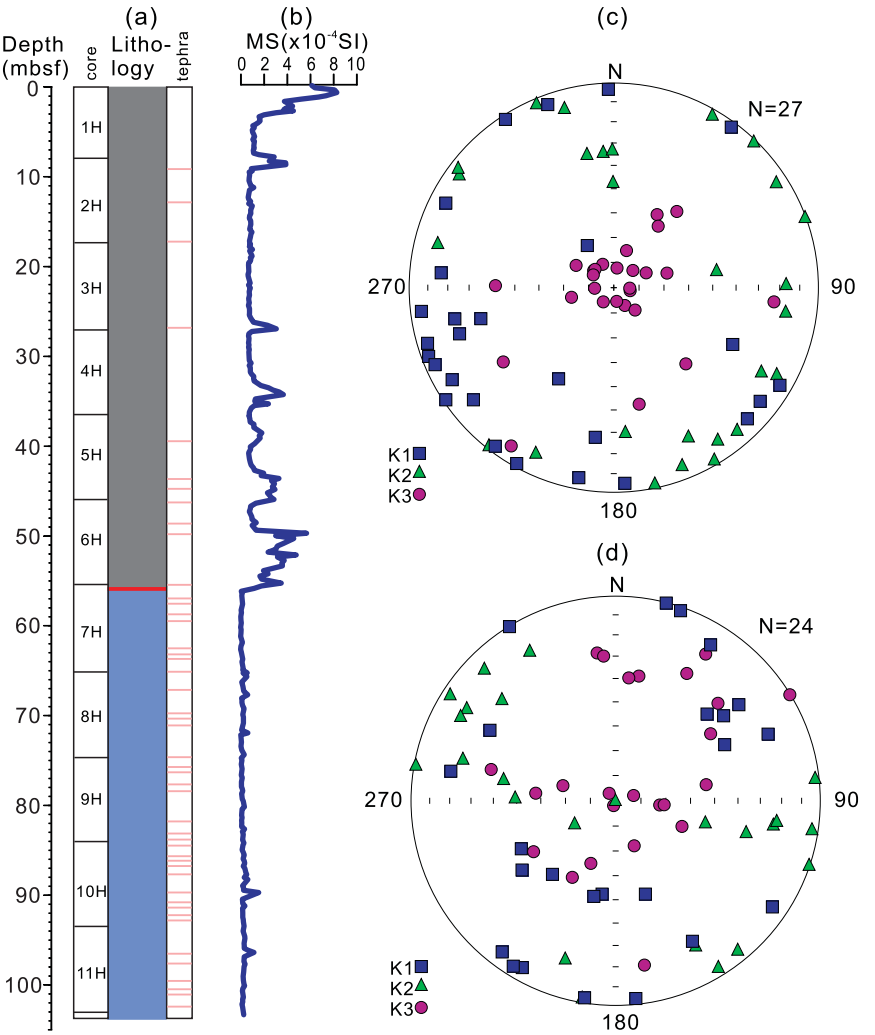


**Figure 3.** The lithology and magnetic susceptibility data of Hole U1381C. (a) Downhole change in lithology from silty clay (gray) to nannofossil ooze (blue); (b) downhole changes in low-field magnetic susceptibility; (c, d) anisotropy of magnetic susceptibility (AMS) data of Hole U1381C. The AMS data in Figure 3c are from the basal 10 m of the upper unit of hemipelagic clays and the AMS data in Figure 3d are from the upper 10 m of the middle unit of pelagic calcareous ooze. k1, k2, and k3 are the principal axes, i.e., maximum, intermediate, and minimum axis of the anisotropy ellipsoid, respectively. Figures 3c and 3d are the stereographic projections of k1, k2, and k3. Pink lines in Figure 3a indicate tephra layers.

layer of claystones capping the basaltic basement. Above the basal unit is a 47.27 m thick predominantly pelagic sequence of dark gray to brown, nannofossil calcareous ooze. The uppermost unit is 55.93 m thick and consists mainly of a monotonous sequence of light gray, hemipelagic silty clay to clay sediments. A sedimentary hiatus is recognized at the contact between the upper and middle unit, and is marked by a sharp, distinct color contrast at the boundary between the two units [*Harris et al*., 2013] (Figures 2d and 3a). The occurrence of the sedimentary hiatus is also supported by paleontologic data. Microfossil data from the upper unit yield a Pleistocene age, whereas microfossils from the middle unit indicate a middle Miocene age, suggesting a ~9–11 Myr hiatus [*Harris et al*., 2013]. Another prominent feature of the sediments is the frequent occurrence of distinct tephra layers. There are 18 and 62 tephra horizons in the upper and middle unit, respectively [*Harris et al*., 2013] (Figure 3a). These tephra layers document the evolution of Galapagos volcanism [*Schindlbeck et al*., 2015]. Tephra layers at 78.20 and 86.48 m below seafloor (mbsf) were dated with $^{40}Ar/^{39}Ar$ chronometry [*Schindlbeck et al*., 2015] and the ages estimated for these two tephra layers can be used as anchoring points for magnetostratigraphic studies.

Site U1414 is located on the flank of the CR and is about 1 km away from the MAT (Figure 1). Drilling at Site U1414 also reached the basaltic basement of the CR at ~380 mbsf (Figure 2e). The sedimentary sequence is much thicker than that at Site U1381 and consists of, from bottom to top, siltstone and sandstone,

calcareous and siliceous oozes, and silty clay and clay (Figure 2e). Inspection of the sediments did not reveal a sedimentary hiatus and microfossil ages also indicate that deposition at Site U1414 was continuous [*Harris et al*., 2013] (Figure 2e).

### 2.2. Sites 1241 and 1242

Sites 1241 and 1242 were drilled on the CR during ODP Leg 202 [*Mix et al*., 2003] (Figure 1). Site 1241 is situated at a ramp on the northern flank of the middle part of the CR (Figure 1). Nearly 450 m of thick pelagic sediments were recovered at Site 1241 (Figure 2b). Microfossil data suggest that the pelagic sediments span from the late Miocene to the Holocene (Figure 2b). At Site 1242 (Figure 1), a 287.74 m thick sedimentary sequence was recovered. The sedimentary sequence comprises two lithologic units (Figure 2c). The lower unit contains pelagic sediments that are dominated by nannofossil ooze and the upper unit is composed of hemipelagic sediments that are dominated by nannofossil clay (Figure 2c). An abrupt lithologic change between the lower and upper unit marks a prominent sedimentary hiatus (Figure 2c). Microfossil ages show that the lower unit is middle Miocene and the upper unit spans from the late Pliocene to the Holocene (Figure 2c).

### 2.3. Sites 844 and 1039

Sites 844 and 1039 were drilled on the Cocos Plate near the CR during ODP Legs 138 and 170, respectively [*Mayer et al*., 1992; *Silver et al*., 2000] (Figure 1). About 290 m of pelagic sediments dominated by biogenic ooze were recovered at Site 844 (Figure 2a). The sedimentary sequence at Site 844 spans from the early Miocene to the Pleistocene [*Mayer et al*., 1992] (Figure 2a). Site 1039 is situated immediately seaward of the MAT [*Silver et al*., 2000] (Figure1). The sedimentary sequence at Site 1039 contains, from bottom to top, calcareous ooze, silty clay, and diatom ooze (Figure 2f). Microfossil ages indicate that the sediments span from the middle Miocene to the Pleistocene [*Silver et al*., 2000] (Figure 2f).

## 3. Laboratory and Analytical Methods

### 3.1. Paleomagnetic Sampling

A total of 398 discrete paleomagnetic samples were taken over the 103.5 m long section from Hole U1381C, yielding an overall average sampling interval of $\sim$25 cm. Because the sediments are mostly unconsolidated, paleomagnetic samples were taken by pushing nonmagnetic 7 $cm^3$ cubes into the split halves of the cores. During sampling, only sediments showing no visible signs of deformation were sampled. All samples were kept in a relatively cold temperature and low magnetic field environment (in magnetically shielded containers) to inhibit water loss and prevent viscous remanence acquisition.

### 3.2. Magnetic Measurement Procedure

The paleomagnetic and rock magnetic data presented in this paper are from measurements performed both on the *JOIDES Resolution* (JR) and in the paleomagnetism laboratory at Nanjing University. To investigate the nature of the remanent magnetization of the rocks from Site U1381, discrete samples were alternating-field (AF) demagnetized during shipboard and shore-based studies to identify magnetic components and to evaluate the directional stability and coercivity spectra of each sample. In the shipboard studies, 85 discrete samples were subjected to stepwise AF demagnetization up to 120 mT in 13 steps using a DTECH D-2000 AF demagnetizer, and the remanence was measured with a 2G Enterprises Inc. 760R superconducting rock magnetometer. In the shore-based studies, low-field magnetic susceptibility (MS) of 313 samples and anisotropy of magnetic susceptibility (AMS) of selected samples were first measured with an AGICO Kappabridges KLY-3. The samples were then subjected to progressive AF demagnetization up to 100 mT at increments of 5 or 10 mT using a Molspin demagnetizer. Remanence was measured with a 2G Enterprises Inc. 755 superconducting rock magnetometer housed in a magnetically shielded room (residual field $<$ 300 nT).

To further characterize the rock magnetic properties, representative samples were subjected to several additional magnetic measurements. Curie temperatures were determined by measurement of low-field magnetic susceptibility versus temperature using the CS4 apparatus attached to the Kappabridge susceptibility meter (MFK1) at the Paleomagnetism and Geochronology laboratory at Institute of Geology and Geophysics, Chinese Academy of Science. To avoid oxidation that could lead to chemical alteration, we conducted thermomagnetic analyses in an inert argon atmosphere. To determine the Curie temperature, we used a graphic method [*Grommé et al*., 1969] that utilizes the intersection of two tangents to the

thermomagnetic curve that bounds the Curie temperature. This method is simple and straightforward even though it tends to underestimate Curie temperatures compared to more complex methods [*Moskowitz*, 1981; *Tauxe*, 1998]. The results, nonetheless, are sufficient for the purposes of this study.

Isothermal remanent magnetization (IRM) acquisition experiments were conducted using an ASC impulse magnetizer. Selected samples were progressively magnetized in a forward field up to 1.4 T and were then demagnetized in a back DC field. Remanent magnetization was measured between each treatment using a JR-6A spinner magnetometer. Hysteresis loop parameter measurements were performed on a Magnetic Property Measurement System (MPMS) using 50–100 mg sediment samples to estimate the domain state of magnetic particles [*Day et al*., 1977; *Dunlop*, 2002].

### 3.3. Data Analyses

The software Puffinplot [*Lurcock and Wilson*, 2012] was used for analyzing paleomagnetic data obtained at both the JR and Nanjing University paleomagnetism laboratories. Changes in the intensity and direction of remanent magnetization vectors during demagnetization experiments were analyzed using orthogonal vector endpoint projections [*Zijderveld*, 1967]. For samples that gave reliable demagnetization results, magnetization components were determined by fitting least squares lines to segments of the vector demagnetization plots that were linear in three-dimensional space (principal component analysis or PCA) [*Kirschvink*, 1980].

To obtain reliable estimates of the characteristic remanent magnetization from the demagnetization data, we devised the following criteria to avoid overprinted and magnetically unstable samples. First, Site U1381 is located at 8°25.7′N and inclinations of the Earth's magnetic field at the site were around 35° in October 2012 according to the international geomagnetic reference field (IGRF) model (www.ngdc.nova.gov). Since Site U1381 has remained close to the equator in its entire history according to plate reconstructions of the Cocos Plate [*Pisias et al*., 1995] and has not moved further north than its present latitude of 8°25.7′N, the expected inclination of the geocentric axial dipole field at the site should be $\leq$16.5°. As a result, we reject any measurements with inclinations larger than $\pm$70°, which is a likely sign that a drilling-induced magnetic overprint is present [*Acton et al*., 2002; *Zhao et al*., 1994]. Second, we accept samples with Maximum Angular Deviation (MAD) [*Kirschvink*, 1980] angles of mostly anchored PCA analyses that are $<$16°. Third, we generally accept data if the higher coercivity component of a sample shows a linear trend to the origin with at least three data points included in the PCA analysis. Finally, results from samples exhibiting no stable directional endpoint were discarded on the grounds that they were either unstable or heavily contaminated by a drilling-induced remanence that could not be easily removed.

Because the uppermost 84 m (Cores 1H–9H) at Site U1381 are fully oriented and the site is situated at low latitude in the Northern Hemisphere, downhole changes in declinations are used jointly with downhole changes in VGP latitudes to define polarity zones for the uppermost 84 m section. For the lower $\sim$20 m where there is no orientation data, both declinations and inclinations were used to define polarity zones. Because Site U1381 has always been situated in the Northern Hemisphere, positive (downward directed) inclinations are taken to signify a normal polarity, and negative (upward directed) inclinations signify reverse polarity. We correlate polarity zones with the geomagnetic polarity time scale (GPTS) [*Ogg*, 2012] in a manner that appears most consistent with both magnetic and biostratigraphic data. In naming the various polarity intervals, we use the familiar proper names for the Pleistocene magnetic chrons (e.g., Brunhes, Matuyama) and subchrons (e.g., Jaramillo) and the conventional nomenclature [*Cande and Kent*, 1995] for older times.

## 4. Results

### 4.1. Rock Magnetic Results of Hole U1381C

Downhole magnetic susceptibility (MS) variations largely reflect lithologic changes (Figures 3a and 3b). The hemiplegic clay-dominated upper unit has slightly stronger MS than the weaker middle unit, which is dominated by pelagic calcareous ooze. The striking, sharp decrease in MS corresponds to the sedimentary hiatus between the upper and middle unit at 55.93 m (Figures 3a and 3b). Anisotropy of magnetic susceptibility (AMS) data of the basal 10 m of the upper hemipelagic clay unit show a predominantly oblate fabric that is characterized by (1) fairly well grouped minimum axes (k3) largely perpendicular to the bedding, and (2) maximum (k1) and intermediate (k2) axes dispersed in the bedding plane (Figure 3c), indicating a normal depositional fabric. The AMS data of the top 10 m of the pelagic calcareous ooze unit display a weak oblate

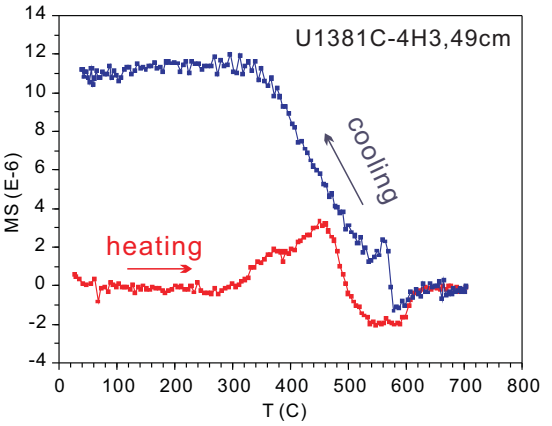


**Figure 4.** Temperature dependence of magnetic susceptibility for a representative sample from the upper unit of hemipelagic clay of Hole U1381C showing changes in magnetic susceptibility during heating and cooling between room temperature and 700°C.

fabric. The minimum axes (k3) are scattered and are not all perpendicular to bedding, whereas the maximum (k1) and intermediate (k2) axes are generally not parallel to bedding (Figure 3d). These features suggest that the original depositional oblate fabrics in the upper part of the middle unit were slightly disturbed, probably during the formation of the sedimentary hiatus.

Thermomagnetic curves of samples from the upper unit of hemipelagic clays show irreversible behavior (Figure 4). The cooling curve is higher than the heating curve at all temperatures, suggesting that a mineralogic transformation took place during heating. The rapid increase in MS at ~580°C during cooling suggests that magnetite was produced during heating. The heating curve peaks at ~500°C and subsequently shows a gradual decay. Using the two-tangent method of *Grommé et al.* [1969] for the heating curve, the Curie temperature of the magnetic minerals is estimated to be ~560°C, suggesting that magnetite and titanomagnetite are probably the primary remanence carriers.

Isothermal remanent magnetization (IRM) data show that the samples are largely saturated by 200 mT (Figures 5a and 5b) and some samples from the upper unit are saturated by 100 mT (Figure 5a), suggesting that low coercivity magnetic phases dominate the samples and reinforcing the results of the thermomagnetic analysis. Back-field demagnetization of the saturated IRM indicates that the remanent coercivity of the hemipelagic clay unit is relatively low, ranging from ~30 to ~70 mT (Figure 5a), whereas the remanent coercivity of the pelagic calcareous ooze unit is relatively high, varying from ~70 to ~120 mT (Figure 5b). The hysteresis loops of two representative samples from the upper and middle unit show that paramagnetic phases are present in both units (Figures 5c and 5d). Removing the contribution from the paramagnetic phases, the loops close at ~150 and ~300 mT (Figures 5c and 5d) for the samples from the upper and middle unit, respectively. Calculation of the $J_r/J_s$ and $H_{cr}/H_c$ ratios indicates that the magnetic grains are in the pseudosingle domain (PSD) range according to the theoretical models of *Day et al.* [1977] and *Dunlop* [2002]. The same PSD results and similar coercivity ranges were obtained from measurements of hysteresis loops and first-order reversal curves (FORCs) of two carbonate ooze samples (57.12 and 57.84 mbsf) and one silty clay sample (49.81 mbsf) from Hole U1381C [*Petronotis et al.*, 2015]. FORC diagrams display characteristics for SD and PSD grains [*Roberts et al.*, 2000], and the range of coercivities suggests that magnetite is the dominant magnetic mineral. In summary, these consistent rock magnetic results suggest that samples from Hole U1381C exhibit stable remanent magnetization with bulk magnetic grain sizes in the PSD region. Therefore, the samples are most likely good paleomagnetic recorders that have preserved an original and stable magnetic remanence.

### 4.2. Paleomagnetic Results of Hole U1381C

The natural remanent magnetization of the samples ranges mainly from $\sim 3.4 \times 10^{-4}$ to $\sim 2.8 \times 10^{-2}$ A/m. Demagnetization of the samples typically exhibits a two-component magnetization (Figure 6). The lower coercivity (<10–15 mT) component is near vertical and represents a drilling-induced magnetization [Acton et al., 2002; Zhao et al., 1994]. The higher coercivity component decays toward the origin and defines the characteristic remanent magnetization (ChRM) of the samples. Of the 398 samples analyzed, 47 samples show erratic directions upon demagnetization and another 59 samples have a ChRM MAD that is >16°. These samples were excluded from constructing a magnetic polarity stratigraphy. Because Site U1381 is located near the equator, declination differences are more diagnostic than variations in inclination in determining a magnetic polarity stratigraphy. Thus, downhole changes in declinations and VGP latitudes were taken together to define a magnetic polarity stratigraphy (Figure 7; supporting information, Dataset S1). A polarity zone is defined based on at least two consecutive data points of the same polarity.

Because there is a sedimentary hiatus between the calcareous ooze and silty clay units (Figures 7a and 7b), the correlation of the polarity stratigraphy to the GPTS was made separately for the lower and upper unit

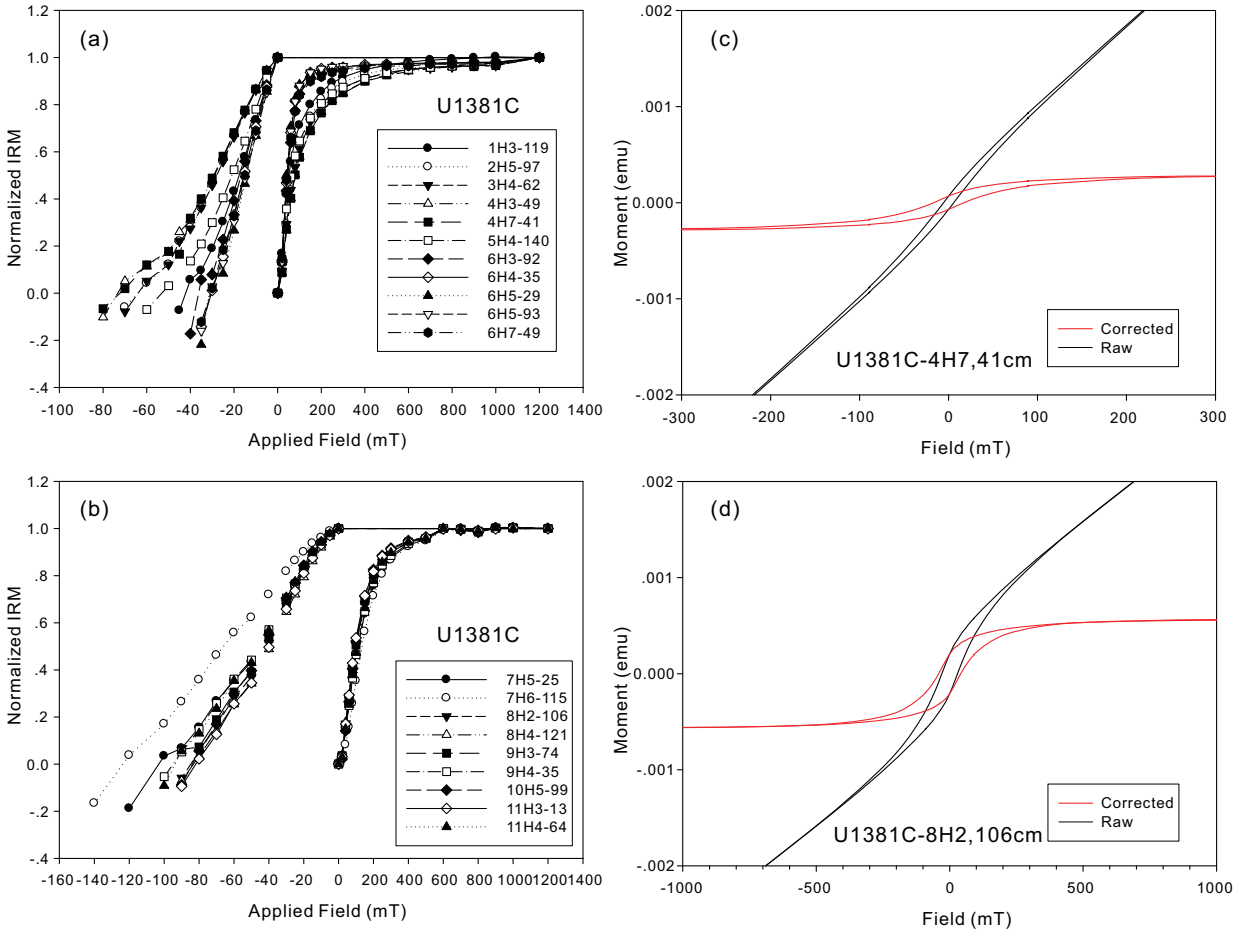


**Figure 5.** (a, b) Isothermal remanent magnetization acquisition and back-field demagnetization, and (c, d) hysteresis loops of selected samples of the upper unit of hemipelagic clay and the middle unit of pelagic calcareous ooze of Hole U1381C.

(Figures 7e and 7f). The normal polarity zones in the upper unit are correlated to the Brunhes Chron, the Jaramillo Subchron, and the Cobb Mountain Subchron, respectively (Figures 7e and 7f). The correlation of the polarity zones in the middle unit is tentative and is facilitated by $^{40}Ar/^{39}Ar$ age determinations of 12.0 ± 1.2 and 13.94 ± 0.015 Ma from two tephra layers at 78.02 and 86.48 mbsf [*Schindlbeck et al*., 2015], respectively, that serve as two anchoring points (Figures 7e and 7f). The longest normal and reverse polarity zones in this unit are thus correlated to Subchrons C5n and C5r, respectively (Figures 7e and 7f). The missing time represented by the hiatus can be estimated from the difference between the basal age of the upper unit and the age of the uppermost part of the middle unit. Within this chronologic framework (Figures 7e and 7f), ages can be approximated by extrapolation of the age-depth relations defined by the magnetic polarity chrons and subchrons in the upper and middle unit, respectively (Figure 8). To obtain a precise basal age of the upper unit, sedimentation rates defined by Subchrons C1r.1r, C1r.1n, C1r.1, and C1r.1+C1r.2 (Figure 7) and the mean sedimentation rates for C1r.1r + C1r.1n and C1r.1 + C1r.2 are averaged. The basal age of the upper unit is thus calculated to be ~1.52 Ma with a standard deviation of ±0.09 Ma. Similarly, for the middle unit, using the sedimentation rates defined by Subchrons C5n, C5r, and C5n+C5r (Figure 7), the age of the upper boundary of the middle unit is calculated to be ~9.605 Ma with a standard deviation of 0.03 Ma. Thus, the hiatus is bracketed between ~9.61 and ~1.52 Ma, representing ~8.09 Myr of missing time.

### 4.3. A Regional Sedimentary Hiatus

To examine the areal extent of the sedimentary hiatus observed at Site U1381, we compare stratigraphic columns at sites from the CR and nearby sites on the Cocos Plate (Figures 2a–2f). To facilitate regional, between-site stratigraphic correlations, the stratigraphic columns of these sites are placed in an order that broadly reflects the distance of each site from the trench (Figures 2a–2f). Sites 844 and 1241 are the two

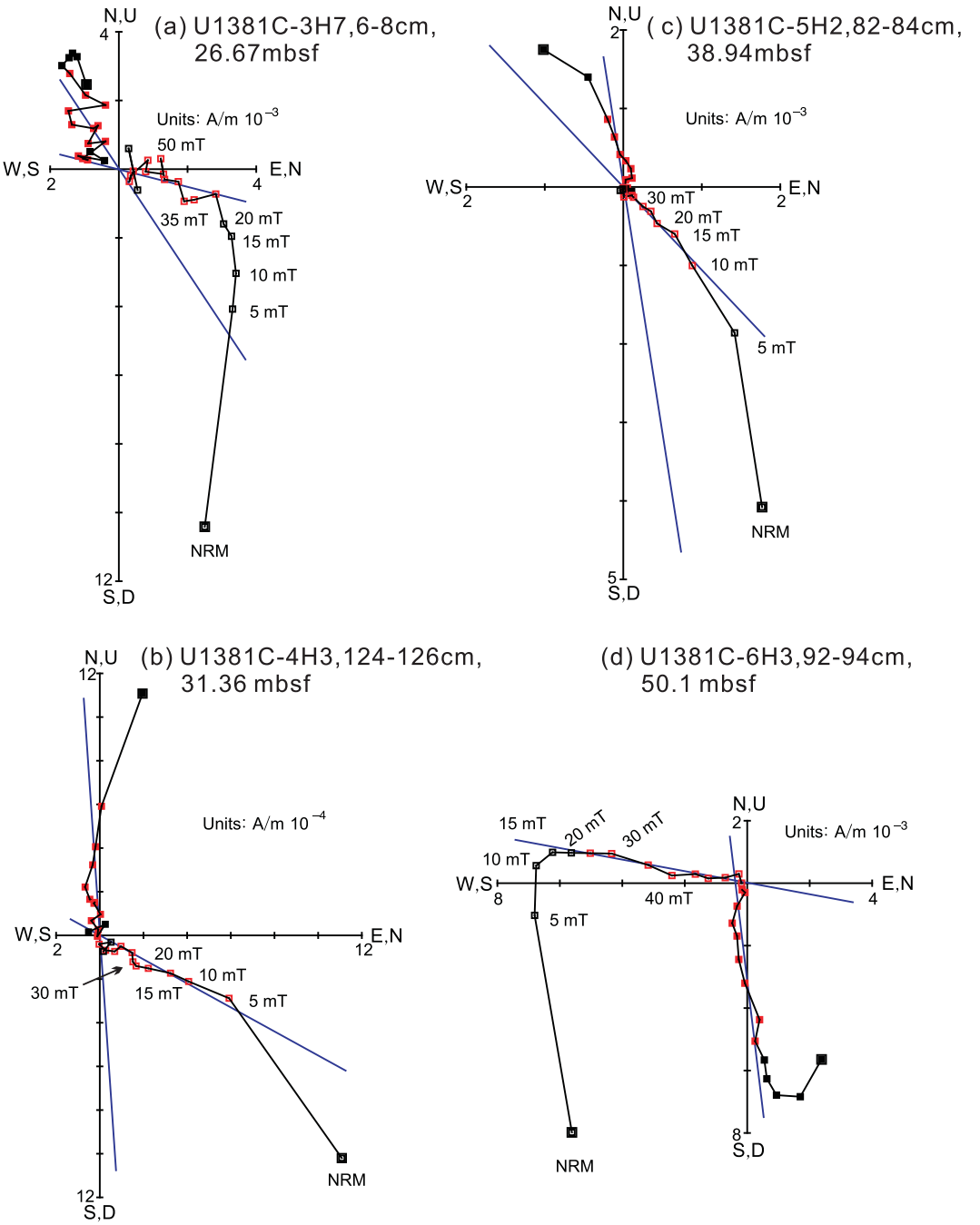


**Figure 6.** Representative vector-end-point plots for AF demagnetization results [*Zijderveld*, 1967]. Solid squares indicate the horizontal magnetization components, and open squares indicate the vertical components. The blue straight lines represent the primary remanence using principal component analysis [*Kirschvink*, 1980]. Sample depths are given as meters below seafloor (mbsf).

most distal sites and are located about 450 km away from the trench. Site 844 is situated on the Cocos Plate, and Site 1241 sits in the middle of the CR (Figure 1). Cores from these two sites consist of pelagic sediments that show little lithologic change (Figures 2a and 2b). Microfossil ages suggest that the ~290 m thick sedimentary section at Site 844 spans from the early Miocene to the Pleistocene and the ~450 m thick sedimentary section at Site 1241 spans from the late Miocene to the Pleistocene.

Sites U1381 and 1242 are located atop the northeastern part of the CR, about 40–50 km away from the MAT (Figure 1). These two sites record a history of hemipelagic sedimentation at the CR. Sediments at both sites are dominated by two units (Figures 2c and 2d). The lower unit consists of nannofossil calcareous ooze

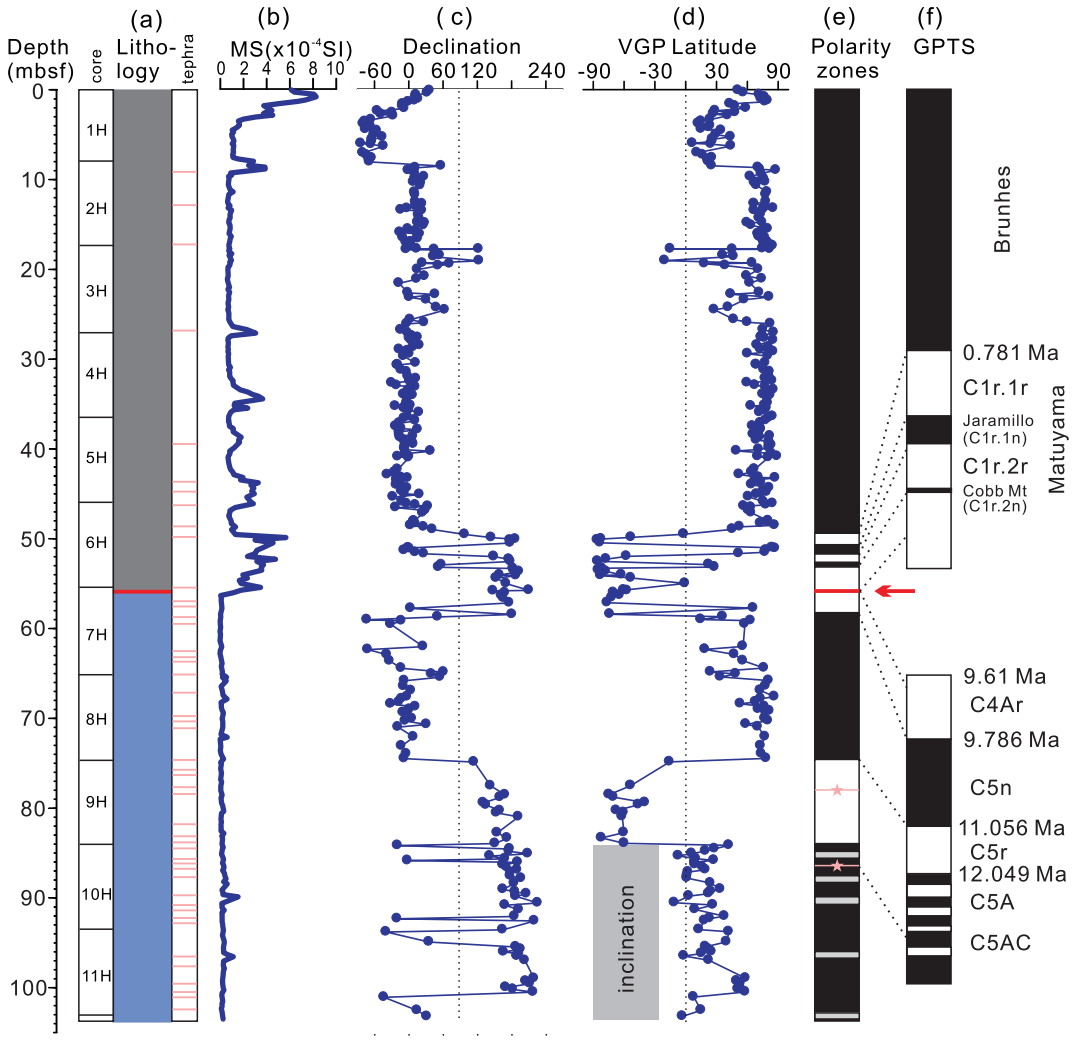


**Figure 7.** Lithology and magnetostratigraphy of Hole U1381C. (a) Lithology; (b) magnetic susceptibility (MS); (c) declination; (d) virtual geomagnetic pole (VGP) latitude except for the lower 20 m (highlighted with a gray rectangle) where inclinations and declinations are shown; (e) polarity zones (black/white = normal/reversed polarity; gray = cores 10H to 11H that were not fully oriented; the red line/arrow indicates the hiatus and the asterisks indicate the tephra layers at which $^{40}Ar/^{39}Ar$ ages were obtained) [*Schindlbeck et al.*, 2015]; (f) geomagnetic polarity time scale (GPTS) [*Ogg*, 2012].

and lacks siliciclastic components. The upper unit comprises predominantly silty clay with generally decreasing biogenic content uphole, probably due to increasing terrigenous input from the exhumed upper plate at the active continental margin setting [*Mix et al.*, 2003; *Harris et al.*, 2013]. The boundary between the lower and upper units is marked by a sharp contact (asterisks in Figures 2c and 2d). Microfossil ages indicate that the sharp contact at Site U1381 represents a ~10 Myr hiatus that corresponds to a missing Pliocene record (Figure 2d) [*Harris et al.*, 2013]. At Site 1242, the hiatus is marked by distinct changes in color and lithology (asterisk in Figure 2c) [*Mix et al.*, 2003]. Based on nannofossil, foraminifer, and diatom biostratigraphy, the hiatus spans from ~3 to 12 Ma and corresponds to a missing late Miocene to Early Pliocene record (Figure 2c) [*Mix et al.*, 2003]. The chronology of the hiatus could not be further constrained due to the lack of high-quality paleomagnetic data from Site 1242 [*Mix et al.*, 2003]. Besides the occurrence of a hiatus at Sites U1381 and 1242, the sedimentary cover at this part of the CR is generally thin. In particular, cores from Site U1381 penetrated through the sedimentary cover into the basaltic basement and the total thickness of the sedimentary cover is only about 100 m (Figure 2d).

Sites U1414 and 1039 are the two most proximal sites to the subduction zone and only a few kilometers away from the MAT (Figure 1). Unlike Site U1381 that is located at the summit of the CR, Site U1414 is situated on the lower flank of the CR. The sedimentary section at Site U1414 consists, from bottom to top, of

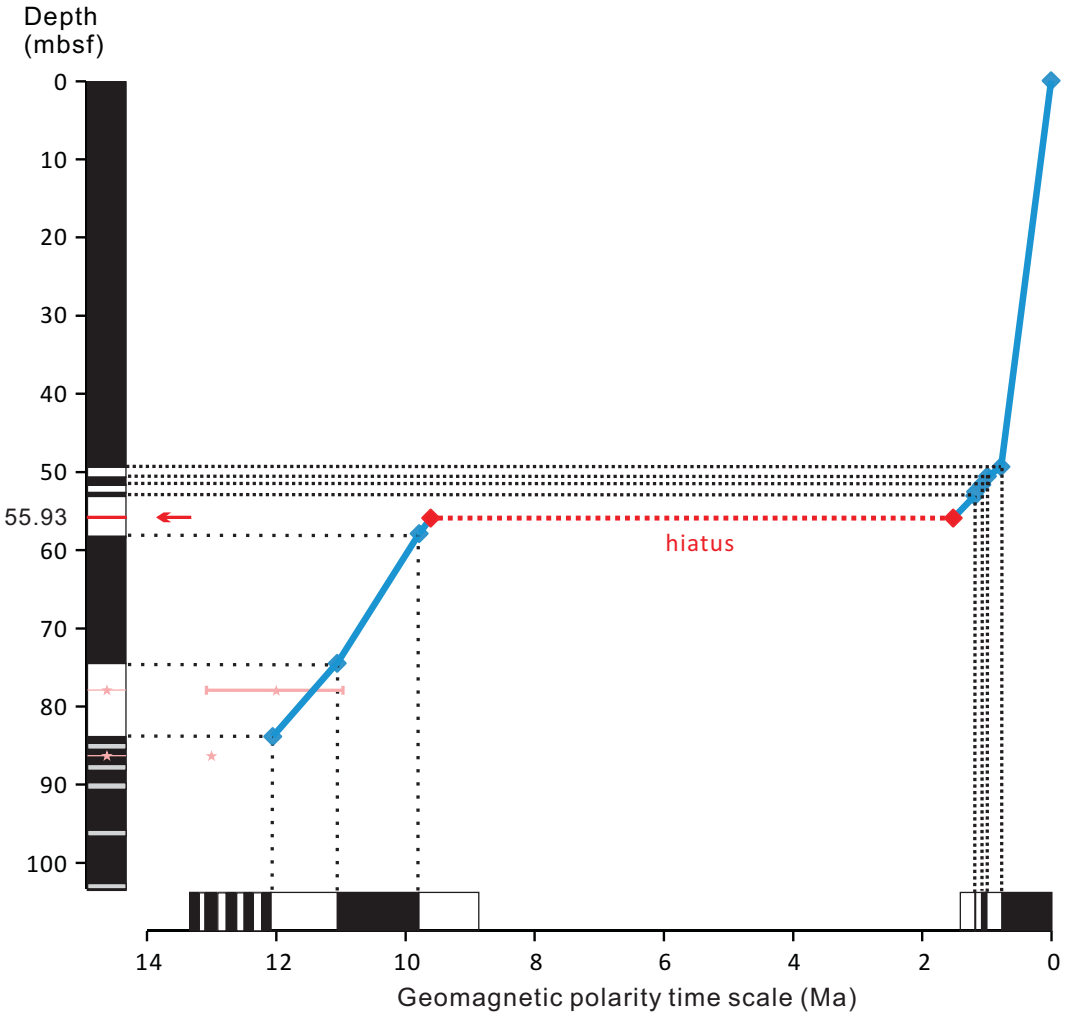


**Figure 8.** Age-depth model of Hole U1381C. The geomagnetic polarity time scale (GPTS) is based on *Ogg* [2012]. mbsf, meter below seafloor. The red arrow and dashed line mark the hiatus. The red diamonds indicate the upper and lower bound ages of the hiatus based on extrapolation. The pink lines with asterisks mark the tephra layers at which $^{40}Ar/^{39}Ar$ ages were obtained [*Schindlbeck et al.*, 2015].

lithified siltstone/sandstone (Unit III), moderately consolidated calcareous ooze (Unit II), and monotonous hemipelagic silty clay to clay (Unit I) (Figure 2e) [*Harris et al.*, 2013]. Both the upper part of Unit II and the lower part of Unit I are nannofossil rich, and microfossil ages do not show a rapid change across the boundary between Unit I and Unit II [*Harris et al.*, 2013], suggesting that the transition from pelagic calcareous ooze to hemipelagic clay at Site U1414 is gradual. Site 1039 is situated on the Cocos Plate and yielded a sedimentary section with nannofossil ooze in the lower part, silty clay in the middle, and diatom-bearing ooze in the upper part (Figure 2f). Microfossil ages suggest the sedimentation is continuous and the record spans from the middle Miocene to the Pleistocene [*Silver et al.*, 2000] (Figure 2f). The sedimentary sequences at both sites are ~400 m thick and are greatly expanded compared to Sites 1242 and U1381, which are located more distant from the MAT.

## 5. Discussion

The results show that the sedimentary hiatus we have identified does not occur everywhere. Sites 844 and 1039 from the Cocos Plate do not show a hiatus. A hiatus occurs on the CR, but appears to be restricted to areas near the convergent margin and also at the top of the CR. The occurrence of the sedimentary hiatus at both Sites 1242 and U1381 suggests that the hiatus is probably a regional feature, spanning the entire northeastern end of the CR (Figures 1 and 2). Furthermore, the absence of the hiatus at Site U1414, located lower on the flank of the CR, suggests that the hiatus is restricted to areas closer to the top of the CR. In addition, it is interesting to note that, along the CR axis, the presence/absence of the sedimentary hiatus

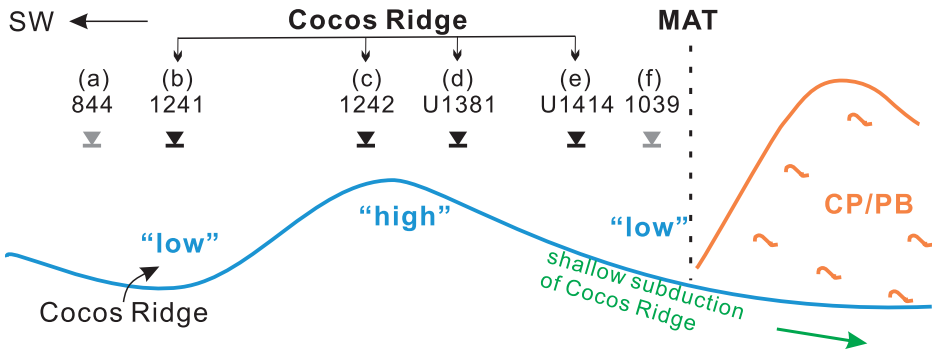


**Figure 9.** The proposed CR buckling model illustrating sedimentary responses to the CR collision with the Middle American Trench (MAT). CP/PB = Caribbean Plate/Panama Block; black/gray triangles indicate sites on the Cocos Ridge/Cocos Plate, respectively.

appears to show a somewhat alternating pattern, i.e., the hiatus is absent from the distal site (Site 1241) and from the site closest to the trench (Site U1414), but is present at sites on the summit and near the trench (Sites 1242 and U1381) (Figures 1 and 2).

The hiatus observed at Site 1242 has been previously postulated to be related to the closure of the Isthmus of Panama and/or local tectonics [*Mix et al.*, 2003]. Had the closure of the Isthmus of Panama caused the hiatus, a hiatus would have been expected in a large area across the Cocos Plate. For example, the sedimentary record at Site 1039 is continuous despite a change from pelagic to hemipelagic sedimentary facies (Figure 2f). The fact that the hiatus occurs only on the northeastern end of the CR near the convergent margin implies that the formation of the hiatus was more likely related to the initial, near-flat subduction of the CR.

Here we propose two possible mechanisms that can link the hiatus to the initial shallow subduction of the CR: bottom current erosion or buckling of the CR.

### 5.1. Bottom Current Erosion

The most straightforward explanation for the hiatus is erosion caused by ocean bottom currents. The absence of the hiatus in areas far away from the trench, such as Site 1241, and the presence of the hiatus near the trench, such as Sites 1242 and U1381, suggest that strong bottom currents were produced near the trench and were probably closely related to the onset of the CR subduction at the MAT. The initial shallow subduction of the CR caused complex interactions between the CR and the fore arc, leading to intense subduction erosion and regional fore-arc subsidence at the Costa Rican convergent margin [e.g., *von Huene et al.*, 2000; *Vannucchi et al.*, 2013]. It is plausible that initial strong margin tectonism could have triggered landslides near the trench, generating strong, focused, sediment-bearing, dense bottom currents near the convergent margin. Together with the rough topography of the CR, bottom currents could have become highly erosive and given rise to the formation of the sedimentary hiatus near the trench. The process is probably similar to that on the Iberian Gulf of Cadiz margin where dense Mediterranean outflow water caused a sedimentary hiatus in some parts of the sedimentary sequence [e.g., *Maldonado and Nelson*, 1999].

### 5.2. Buckling of the CR

Alternatively, the presence of the sedimentary hiatus at Sites 1242 and U1381 and the absence of a hiatus at the other four sites can be explained by buckling of the CR upon its arrival at the MAT. The near-flat subduction and the rough topography of the CR could create strong friction upon its initial collision with the MAT. The frictional force may have been large enough to cause the CR to buckle so that the surface of the basaltic basement undulated along the CR axis and caused a depositional hiatus above the uplifted "high" areas of the basement. In theory, an elastic plate can buckle under a strong horizontal force [*Turcotte and Schubert*, 2002]. Also, physical laboratory modeling can produce flexural buckling of an "oceanic" plate at the initial stage of horizontal compression, mimicking a strong frictional force during subduction [*Shemenda*, 1992, Figure 8]. Therefore, it is possible that the CR buckled upon its initial collision with the MAT.

The occurrence/absence of a sedimentary hiatus at certain distance from the trench is consistent with the CR buckling model (Figure 9). Sites 1242 and U1381 sit on the upwarped "high" (Figures 2 and 9), documenting a hemipelagic deposition and recording the sedimentary hiatus. Site 1241 is located behind the upwarp "high" in the seaward downwarp "low," where thickened, continuous pelagic sediments accumulated (Figures 2

and 9). Finally, Site U1414 documents sedimentation at the landward downwarp "low" where thickened, continuous hemipelagic sediments with abundant terrigenous components were deposited (Figures 2 and 9). Sites 844 and 1039 record essentially continuous Cocos Plate deposition, away from the tectonic effects of the CR.

Paleomagnetic results show that the hiatus was formed prior to 1.52 Ma (Figure 7). This age is consistent with the estimated timing [e.g., *Vannucchi et al.*, 2013] of the initial collision of the CR and the MAT. The uplift of the upper plate associated with the CR subduction is constrained at <3.0 Ma [*Morell et al.*, 2012]. A 2–3 Ma age for the incipient subduction of the CR [*MacMillan et al.*, 2004] is inferred based on the plate tectonic reconstruction of the southern central American volcanic arc. Recent analysis of the fore-arc evolution reveals a significant fore-arc subsidence episode at 2.3–1.9 Ma that is thought to result from subduction erosion during CR subduction [*Vannucchi et al.*, 2013]. The compatible ages between the hiatus formation and the margin tectonism associated with the initial CR subduction strengthen the inference that the hiatus is probably associated with the initial intense tectonism at the Costa Rican convergent margin upon the arrival of the CR.

## 6. Conclusions

Sedimentary records of four ODP/IODP sites (1241, 1242, U1381, and U1414) from the Cocos Ridge and two nearby ODP sites (844 and 1039) are compiled and analyzed. Continuous deposition is found at Sites 1241, 844, U1414, and 1039, whereas a sedimentary hiatus is recognized in the hemipelagic successions at Sites 1241 and U1381, which are located about 10–50 km away from the trench on the northeastern part of the CR. The hiatus is probably regional in extent and spans over the whole northeastern end of the CR.

A detailed paleomagnetic study was carried out on sedimentary cores from Site U1381 that were mostly fully oriented. A polarity time scale is established and the hiatus is constrained between ~9.61 and ~1.52 Ma, representing ~8.09 Myr of missing time. The lower age estimate indicates that the initial strong margin tectonism must have been completed by ~1.52 Ma.

The origin of the sedimentary hiatus is probably tectonic related. The hiatus can be explained by either (1) bottom current erosion associated with landslides due to intense tectonic interactions between the shallowly subducting CR and the fore arc, or (2) buckling of the CR upon its initial collision with the MAT. The age of the hiatus formation is consistent with the estimated timing for the initial CR collision at the MAT and the intense tectonic interaction with the Costa Rica fore arc. In essence, this study highlights the tectonic origin of the sedimentary hiatus and emphasizes that sedimentary records obtained from the CR can provide a new window into understanding the geodynamic evolution of the central American convergent margin.

**Acknowledgments**

We are grateful to the crew and technical staff of *JOIDES Resolution* Expedition 344 for their efforts during this expedition. We would like to thank Paola Vannucchi for commenting on an earlier version of the manuscript and the reviewers for their constructive comments that helped improve the manuscript. The manuscript also benefited from fruitful discussions with Jason Morgan, Alex Webb, and Xiumian Hu, for which we express our thanks. This study used data and samples provided by the Integrated Ocean Drilling Program (IODP), and was supported by IODP-China (2008AA09300), National Natural Science Foundation of China (41476029), the Fundamental Research Funds for the Central Universities (20620140389), U.S. National Science Foundation (EAR-1250444), and Fundação Coordenação de Aperfeiçoamento de Pessoal de Nível Superior–CAPES.

## References

Abratis, M., and G. Wörner (2001), Ridge collision, slab-window formation, and the flux of Pacific asthenosphere into the Caribbean realm, *Geology*, *29*, 127–130, doi:10.1130/0091-7613.

Acton, G. D., M. Okada, B. M. Clement, S. P. Lund, and T. Williams (2002), Paleomagnetic overprints in ocean sediment cores and their relationship to shear deformation caused by piston coring, *J. Geophys. Res.*, *107*(B4), doi:10.1029/2001JB000518.

Barckhausen, U., C. R. Ranero, R. von Huene, S. C. Cande, and H. A. Roeser (2001), Revised tectonic boundaries in the Cocos plate off Costa Rica: Implications for the segmentation of the convergent margin and for plate tectonic models, *J. Geophys. Res.*, *106*(19), 19,207–19,220, doi:10.1029/2001JB000238.

Cande, S. C., and D. V. Kent (1995), Revised calibration of the geomagnetic polarity timescale for the late Cretaceous and Cenozoic, *J. Geophys. Res.*, *100*(B4), 6093–6095.

Corrigan, J., P. Mann, and J. Ingle (1990), Forearc response to subduction of the Cocos Ridge, Panama–Costa Rica, *Geol. Soc. Am. Bull.*, *102*, 628–652, doi:10.1130/0016-7606(1990)102 < 0628:FRTSOT>2.3.CO;2.

Day, R., M. Fuller, and V. A. Schmidt (1977), Hysteresis properties of titanomagnetites: Grain-size and compositional dependence, *Phys. Earth Planet. Inter.*, *13*, 260–267, doi:10.1016/0031-9201(77)90108-X.

DeMets, C., R. G. Gordon, D. F. Argus, and S. Stein (1994), Effect of recent revisions to the geomagnetic reversal time scale on estimates of current plate motions, *Geophys. Res. Lett.*, *21*(20), 2191–2194, doi:10.1029/94GL02118.

Dickinson, W. R., and W. S. Snyder (1978), Plate tectonics of the Laramide Orogeny, in *Laramide Folding Associated With Basement Block Faulting in the Western United States*, edited by V. Matthews, *Geol. Soc. Am. Mem.*, 151, 355–366.

Drummond, M. S., M. Bordelon, J. Z. De Boer, and M. J. Defant (1995), Igneous petrogenesis and tectonic setting of plutonic and volcanic rocks of the Cordillera de Talamanca, Costa Rica-Panama, Central American Arc, *Am. J. Sci.*, *295*, 875–919, doi:10.1130/SPE295-p35.

Dunlop, D. (2002), Theory and application of the Day plot (Mrs/Ms versus Hcr/Hc): 1. Theoretical curves and tests using titanomagnetite data, *J. Geophys. Res.*, *107*(B3), 2056, doi:10.1029/2001JB000486.

Fisher, D. M., T. W. Gardner, P. Sak, J. D. Sanchez, K. Murphy, and P. Vannucchi (2004), Active thrusting in the inner forearc of an erosive convergent margin, Pacific coast, Costa Rica, *Tectonics*, *23*, TC2007, doi:10.1029/2002TC001464.

Gardner, T. W., D. Verdonck, N. M. Pinter, R. Slingerland, K. P. Furlong, T. F. Bullard, and S. G. Wells (1992), Quaternary uplift astride the aseismic Cocos Ridge, Pacific coast, Costa Rica, *Geol. Soc. Am. Bull.*, *104*, 219–232, doi:10.1130/0016-7606(1992)104 <0219:QUATAC>2.3.CO;2.

Gardner, T. W., D. M. Fisher, K. D. Morell, and M. L. Cupper (2013), Upper-plate deformation in response to flat slab subduction inboard of the aseismic Cocos Ridge, Osa Peninsular, Costa Rica, *Lithosphere*, *5*, 247–264, doi:10.1130/L251.1.

Gräfe, K., W. Frisch, I. Villa, and M. Meschede (2002), Geodynamic evolution of southern Costa Rica related to low angle subduction of the Cocos Ridge: Constraints from thermochronology, *Tectonophysics*, *348*, 187–204, doi:10.1016/S0040-1951(02)00113-0.

Grommé, C. S., T. L. Wright, and D. L. Peck (1969), Magnetic properties and oxidation of iron-titanium oxide minerals in Alae and Makaopuhi lava lakes, Hawaii, *J. Geophys. Res.*, *74*(22), 5277–5294.

Harris, R. N., A. Sakaguchi, K. Petronotis, and the Expedition 344 Scientists (2013), *The Proceedings of the Integrated Ocean Drilling Program, Expedition 344, Costa Rica Seismogenesis Project, Program A Stage 2 (CRISP-A2)*, vol. 344, Integrated Ocean Drilling Program, College Station, Tex., doi:10.2204/iodp.proc.344.2013

Hey, R., G. S. Johnson, and A. Lowrie (1977), Recent plate motions in the Galapagos area, *Geol. Soc. Am. Bull.*, *88*, 1385–1403.

Ibaraki, M. (2000), Planktonic foraminifers off Costa Rica in the East Pacific Ocean—Biostratigraphic and chronostratigraphic analyses, Proc. Ocean Drill. *Program Sci. Results*, *170*, 1–58.

Kirschvink, J. L. (1980), The least-squares line and plane and the analysis of paleomagnetic data, *Geophys. J. Int.*, *62*, 699–718, doi:10.1111/j.1365-246X.1980.tb02601.x.

Kobayashi, D., P. LaFemina, H. Geirsson, E. Chichaco, A. A. Abrego, H. Mora, and E. Camacho (2014), Kinematics of the western Caribbean: Collision of the Cocos Ridge and upper plate deformation, *Geochem. Geophys. Geosyst.*, *15*, 1671–1683, doi:10.1002/2014GC005234.

LaFemina, P., T. H. Dixon, R. Govers, E. Norabuena, H. Turner, A. Saballos, G. Mattioli, M. Protti, and W. Strauch (2009), Fore-arc motion and Cocos Ridge collision in Central America, *Geochem. Geophys. Geosyst.*, *10*, Q05S14, doi:10.1029/2008GC002181.

Li, Z. X., and X. H. Li (2007), Formation of the 1300-km-wide intracontinental orogen and postorogenic magmatic province in Mesozoic South China: A flat-slab subduction model, *Geology*, *35*, 179–182.

Lonsdale, P., and K. D. Klitgord (1978), Structure and tectonic history of the eastern Panama Basin, *Geol. Soc. Am. Bull.*, *89*, 981–999, doi:10.1130/0016-7606(1978)89<981:SATHOT>2.0.CO;2.

Lurcock, P. C., and G. S. Wilson (2012), PuffinPlot: A versatile, user-friendly program for paleomagnetic analysis, *Geochem. Geophys. Geosyst.*, *13*, Q06Z45, doi:10.1029/2012GC004098.

MacMillan, I., P. B. Gans, and G. Alvarado (2004), Middle Miocene to present plate tectonic history of the southern Central American Volcanic Arc, *Tectonophysics*, *392*, 325–348, doi:10.1016/j.tecto.2004.04.014.

Maldonado, A., and C. H. Nelson (1999), Interaction of tectonic and depositional processes that control the evolution of the Iberian Gulf of Cadiz margin, *Mar. Geol.*, *155*, 217–242.

Mayer, L., N. Pisias, T. Janecek, et al. (1992), 9. Site 844, Proc. Ocean Drill. Program Initial Rep., *138*, 119–188.

Mix, A. C., R. Tiedemann, P. Blum, et al. (2003), 12. Site 1241 and 13. Site 1242, Proc. Ocean Drill. Program Initial Rep., *202*.

Morell, K. D., E. Kirby, D. M. Fisher, and M. van Soest (2012), Geomorphic and exhumational response of the Central American Volcanic Arc to Cocos Ridge subduction, *J. Geophys. Res.*, *117*, B04409, doi:10.1029/2011JB008969.

Morris, J. D., H. W. Villinger, and A. Klaus (Eds.) (2006), 14. Calcareous nannofossil biostratigraphy: Ocean drilling program leg 205, Costa Rica subduction zone, Proc. Ocean Drill. Program Sci. Results, 205.

Moskowitz, M.B. (1981), Methods for estimating Curie temperatures of titanomagnetites from experimental Js-T data, *Earth Planet. Sci. Lett.*, *52*, 84–88.

Newman, A. V., S. Y. Schwartz, V. Gonzalez, H. R. DeShon, J. M. Protti, and L. M. Dorman (2002), Along-strike variability in the seismogenic zone below Nicoya Peninsula, Costa Rica, *Geophys. Res. Lett.*, *29*(20), 1977, doi:10.1029/2002GL015409.

Ogg, J. G. (2012), Chapter 5: Geomagnetic polarity time scale, in *The Geologic Time Scale 2012*, edited by F. M. Gradstein et al., pp. 85–113, Elsevier, Amsterdam, Netherlands.

Petronotis, K. E., G. D. Acton, L. Jovane, Y. X. Li, and X. Zhao (2015), Data report: Magnetic properties of sediments and basalts from the Costa Rica subduction margin (Expeditions 334 and 344), in *Proceedings of Integrated Ocean Drilling Program*, vol. 344, edited by R. N. Harris, A. Sakaguchi, K. Petronotis, and the Expedition 344 Scientists, Integrated Ocean Drilling Program, College Station, Tex., doi:10.2204/iodp.proc.344.206.2015

Pisias, N. G., L. A. Mayer, and A. C. Mix (1995), Paleoceanography of the eastern equatorial Pacific during the Neogene: Synthesis of Leg 138 drilling results, Proc. Ocean Drill. *Program Sci. Results*, *138*, 5–21.

Protti, M., F. Güendel, and K. McNally (1995), Correlation between the age of the subducting Cocos plate and the geometry of the Wadati-Benioff zone under Nicaragua and Costa Rica, in *Geologic and Tectonic Development of the Caribbean Plate Boundary in Southern Central America*, edited by P. Mann, Geol. Soc. Am. Spec. Pap., 295, 309–326.

Ranero, C. R., and R. von Huene (2000), Subduction erosion along the Middle America convergent margin, *Nature*, *404*, 748–752.

Roberts, A. P., C. R. Pike, and K. L. Verosub (2000), First-order reversal curve diagrams: A new tool for characterizing the magnetic properties of natural samples, *J. Geophys. Res.*, *105*(B12), 28,461–28,475, doi:10.1029/2000JB900326.

Sak, P. B., D. M. Fisher, T. W. Gardner, J. S. Marshall, and P. C. LaFemina (2009), Rough crust subduction, forearc kinematics, and Quaternary uplift rates, Costa Rican segment of the Middle American Trench, *Geol. Soc. Am. Bull.*, *121*(7/8), 992–1012, doi:10.1130/B26237.1.

Schindlbeck, J. C., S. Kutterolf, A. Freundt, S. M. Straub, K.-L. Wang, M. Jegen, S. R. Hemming, A. T. Baxter, and M. I. Sandoval (2015), The Miocene Galápagos ash layer record of Integrated Ocean Drilling Program Site U1381: Ocean-island explosive volcanism during plume-ridge interaction, *Geology*, *43*(7), 599–602, doi:10.1130/G36645.1.

Shemenda, A. (1992), Horizontal Lithosphere Compression and Subduction: Constraints provided by physical modeling, *J. Geophys. Res.*, *97*(B7), 11,097-11,116.

Silver, E. A., G. Kimura, and T. H. Shipley (Eds.) (2000), 1. Planktonic foraminifers off Costa Rica in the east pacific ocean—biostratigraphic and chronostratigraphic analyses, Proc. Ocean Drill. Program Sci. Results, 170.

Tauxe, L. (1998), *Paleomagnetic Principles and Practice*, Kluwer Acad, Dordrecht, Boston.

Turcotte, D. L., and G. Schubert (2002), *Geodynamics*, 2nd ed., Cambridge Univ. Press, Cambridge, England.

Vannucchi, P., D. W. Scholl, M. Meschede, and K. McDougall (2001), Tectonic erosion and consequent collapse of the Pacific margin of Costa Rica: Combined implications from ODP Leg 170, seismic offshore data, and regional geology of the Nicoya Peninsula, *Tectonics*, *20*(5), 649–668.

Vannucchi, P., D. M. Fisher, S. Bier, and T. W. Gardner (2006), From seamount accretion to tectonic erosion: Formation of Osa mélange and the effects of Cocos Ridge subduction in southern Costa Rica, *Tectonics*, *25*, TC2004, doi:10.1029/2005TC001855.

Vannucchi, P., K. Ujiie, N. Stroncik, A. Malinverno, and the Expedition 334 Scientists (2012), *Expedition 334 Costa Rica Seismogenesis Project, Program A Stage 1 (CRISP-A1)*, vol. 334, Integrated Ocean Drilling Program, College Station, Tex., doi:10.2204/iodp.proc.334.2012.

Vannucchi, P., P. B. Sak, J. P. Morgan, K. Ohkushi, K. Ujiie, and the IODP Expedition 334 Shipboard Scientists (2013), Rapid pulses of uplift, subsidence, and subduction erosion offshore Central America: Implications for building the rock record of convergent margins, *Geology*, *41*, 995–998, doi:10.1130/G34355.1.

von Huene, R., C. R. Ranero, W. Weinrebe, and K. Hinz (2000), Quaternary convergent margin tectonics of Costa Rica, segmentation of the Cocos Plate, and Central American volcanism, *Tectonics*, *19*(2), 314–334, doi:10.1029/1999TC001143.

Walther, C. H. E. (2003), The crustal structure of the Cocos Ridge off Costa Rica, *J. Geophys. Res.*, *108*(B3), 2136, doi:10.1029/2001JB000888.

Zhao, X., P. Roperch, and L. Stokking (1994), Magnetostratigraphy of the North Aoba Basin, Proc. Ocean Drill. *Program Sci. Results*, *134*, 457–474.

Zijderveld, J. D. A. (1967), A. C. demagnetization of rocks: Analysis of results, in *Methods in Palaeomagnetism*, edited by D. W. Collinson, K. M. Creer, and S. K. Runcorn, pp. 254–286, Elsevier, Amsterdam, Netherlands.

## Erratum

In the originally published version of this article, several references were incorrect. The following have since been corrected and this version may be considered the authoritative version of record.

In the reference section, *Harris et al.* [2013] was corrected.

Harris, R. N., A. Sakaguchi, K. Petronotis, and the Expedition 344 Scientists (2013), *The Proceedings of the Integrated Ocean Drilling Program, Expedition 344, Costa Rica Seismogenesis Project, Program A Stage 2 (CRISP-A2)*, vol. 334, Ocean Drill. Program, College Station, Tex., doi:10.2204/iodp.proc.344.2013

was changed to:

Harris, R. N., A. Sakaguchi, K. Petronotis, and the Expedition 344 Scientists (2013), *The Proceedings of the Integrated Ocean Drilling Program, Expedition 344, Costa Rica Seismogenesis Project, Program A Stage 2 (CRISP-A2)*, vol. 344, Integrated Ocean Drilling Program, College Station, Tex., doi:10.2204/iodp.proc.344.2013

In the reference section, *Petronotis et al.* [2015] was corrected.

Petronotis, K. E., G. D. Acton, L. Jovane, Y. X. Li, and X. Zhao (2015), Data report: Magnetic properties of sediments and basalts from the Costa Rica subduction margin (Expeditions 334 and 344), in *Proceedings of Ocean Drilling Program*, vol. 334, edited by A. Sakaguchi, K. Petronotis, and the Expedition 344 Scientists, Ocean Drill. Program, College Station, Tex., doi:10.2204/iodp.proc.344.206.2015

was changed to:

Petronotis, K. E., G. D. Acton, L. Jovane, Y. X. Li, and X. Zhao (2015), Data report: Magnetic properties of sediments and basalts from the Costa Rica subduction margin (Expeditions 334 and 344), in *Proceedings of Integrated Ocean Drilling Program*, vol. 344, edited by R. N. Harris, A. Sakaguchi, K. Petronotis, and the Expedition 344 Scientists, Integrated Ocean Drilling Program, College Station, Tex., doi:10.2204/iodp.proc.344.206.2015

In the reference section, *Vannucchi et al.* [2012] was corrected.

Vannucchi, P., K. Ujiie, N. Stroncik, A. Malinverno, and the Expedition 334 Scientists (2012), Expedition 334 Costa Rica Seismogenesis Project, Program A Stage 1 (CRISP-A1), vol. 334, Ocean Drill. Program, College Station, Tex., doi:10.2204/iodp.proc.334.2012.

was changed to:

Vannucchi, P., K. Ujiie, N. Stroncik, A. Malinverno, and the Expedition 334 Scientists (2012), Expedition 334 Costa Rica Seismogenesis Project, Program A Stage 1 (CRISP-A1), vol. 334, Integrated Ocean Drilling Program, College Station, Tex., doi:10.2204/iodp.proc.334.2012.